Mutant structure of metabolic switch protein in complex with monomeric c-di-GMP reveals a potential mechanism of protein mediated ligand dimerization

Badri Nath Dubey[1,2]*, Viktoriya Shyp[1,3,4], Geoffrey Fucile[5], Holger Sondermann[2,6], Urs Jenal[1] and Tilman Schirmer[1]

[1] Biozentrum, University of Basel, CH-4056 Basel, Switzerland

[2] CSSB Centre for Structural Systems Biology, Deutsches Elektronen-Synchrotron DESY, Notkestr. 85, 22607 Hamburg, Germany

[3] Department Research, University Center for Dental Medicine Basel UZB, University of Basel, Basel, Switzerland

[4] Department of Oral Health & Medicine, University Center for Dental Medicine Basel UZB, University of Basel, Basel, Switzerland

[5] sciCORE Center for Scientific Computing, University of Basel, CH-4056 Basel, Switzerland

[6] Christian-Albrechts-Universität zu Kiel, Kiel, Germany

* For correspondence: badri.nath.dubey@desy.de

Abstract

Bacterial second messengers c-di-GMP and (p)ppGpp have broad functional repertoires ranging from growth and cell cycle control to the regulation of biofilm formation and virulence. The recent identification of SmbA, an effector protein from *Caulobacter crescentus* that is jointly targeted by both signaling molecules, has opened up studies on how these global bacterial networks interact. C-di-GMP and (p)ppGpp compete for the same SmbA binding site, with a dimer of the c-di-GMP inducing a conformational change that involves loop 7 of the protein thats leads to downstream signaling. Here, we report a crystal structure of a partial loop 7 deletion mutant, SmbA$_{\Delta loop}$ in complex with c-di-GMP determined at 1.4 Å resolution. SmbA$_{\Delta loop}$ binds monomeric c-di-GMP indicating that loop 7 is required for c-di-GMP dimerization. Thus the complex probably represents the first step of consecutive c-di-GMP binding to form intercalated dimer as has been observed in wild-type SmbA. . Considering the prevalence of intercalated c-di-GMP molecules observed bound to proteins, the proposed mechanism may be generally applicable to protein-mediated c-di-GMP dimerization. Notably, in the crystal, SmbA$_{\Delta loop}$ forms a 2-fold symmetric dimer via isologous interactions with the two symmetric halves of c-di-GMP. Structural comparisons of SmbA$_{\Delta loop}$ with wild-type SmbA in complex with dimeric c-di-GMP or ppGpp support the idea that loop 7 is critical for SmbA function by interacting with downstream partners. Our results also underscore the flexibility of c-di-GMP, to allow binding to the symmetric SmbA$_{\Delta loop}$ dimer interface. It is envisaged that such isologous interactions of c-di-GMP could be observed in hitherto unrecognized targets.

Introduction

In all domains of life, second messenger signaling is essential to modulate the intracellular response to external stimuli. In bacteria, purine nucleotide second messengers, such as guanosine tetra- and pentaphosphate, collectively referred to as (p)ppGpp, and bis-(3′-5′)-cyclic dimeric guanosine monophosphate, c-di-GMP, are involved in the global control of physiological responses to environmental change[1,2]. (p)ppGpp is the primary regulator of bacterial growth and development in response to stress and nutrient limitation also known as the stringent response[3,4 5]. It modulates cellular reprogramming via multiple target proteins including RNA polymerase, translational GTPases, and metabolic enzymes[6 7], thereby controlling bacterial transcription, translation[8], cell cycle progression[9 10] stress resistance, and virulence[11 12]. In most bacteria, c-di-GMP controls the transition between motile and sessile lifestyles. Low c-di-GMP levels are associated with motility, while its accumulation promotes adhesion and biofilm formation[13–16] . However, an increasing number of studies indicate that c-di-GMP has an impact on diverse aspects of bacterial physiology including cell cycle progression, metabolism, stress resistance[2,17–22].

The pleiotropic effects of (p)ppGpp and c-di-GMP are realized due to the diversity of their effectors, represented mainly by nucleotide-binding proteins and riboswitches[15,23,24]. In particular, the structural diversity of the cyclic nucleotide, comprising various conformations from an extended monomeric form to a stacked dimer, explains the variety in c-di-GMP-binding motifs[25–27]. The canonical c-di-GMP binding sites are represented by RxxxR and [DN]xSxxG motif in the PilZ domains, RxxD motif in degenerate GGDEF I site of DGCs and ExLxR in the EAL domains of PDEs. Moreover, several proteins with a non-canonical c-di-GMP binding motif have been recently characterized as high-affinity binding receptors, suggesting a widespread function of c-di-GMP in bacteria[25,28].

The development of biochemical methods to identify second messenger effectors greatly complemented our knowledge of novel c-di-GMP and/or (p)ppGpp binding proteins and their interaction networks[28–30]. Recently we have identified the first common target of c-di-GMP and ppGpp, SmbA protein from *C. crescentus*[31]. SmbA stimulates *Caulobacter* growth on glucose while preventing surface attachment in its active state repressed by binding of the c-di-GMP dimer (Fig. 1). The two ligands inversely regulate protein activity presumably by affecting its conformation. The major conformational changes promoting SmbA functional switch affect the C-terminal helix 9 and the flexible loop 7 containing c-di-GMP subsite residues R211 and D214 from the RxxD motif (Fig. 1). In the c-di-GMP-bound state, C-terminal helix 9 is stabilized by a salt bridge of D218 (from the loop7) and R289 (from helix 9), while in the ppGpp-bound state, loop 7 is disordered and helix 9 is in the open conformation (Fig. 1). Mutation of R211 to alanine leads to a prolonged adaptation phase and reduced growth in cells suggesting the involvement of loop 7 and potentially helix 9 in downstream signaling[31].

To date, our structural knowledge about SmbA, however, is restricted to the wild-type protein in the presence of ligands. To understand how flexible loop7 influences the overall SmbA structure and its ligand binding, we present here the high-resolution structure of a loop 7 deletion mutant (fragment 198-215, hereafter SmbA$_{\Delta loop}$). We observe that the mutant retains the TIM-barrel fold, however, accommodates only a monomer of c-di-GMP in a unique extended/open conformation. Importantly, in SmbA$_{\Delta loop}$ mutant, C-terminal helix 9 adopts an outward orientation similar to that found in ppGpp-bound active state protein. Moreover, changes in c-di-GMP binding stoichiometry in SmbA$_{\Delta loop}$ mutant,

120 similar to loop 7 single mutant R211A, provide a potential mechanism and essential role of loop 7 in c-
121 di-GMP dimerization and SmbA functional regulation.

122

Results and discussion

SmbA$_{\Delta loop}$ forms a crystallographic dimer mediated by monomeric c-di-GMP

125 Ligand-induced conformational changes may be critical for SmbA physiological function, in particular
126 for interaction with its yet-to-be-discovered downstream targets. Based on the fact that loop7 is
127 disordered in the apo-state but becomes ordered upon binding of a c-di-GMP dimer, and that mutation
128 of the interacting arginine residue 211 from this loop renders SmbA inactive in signaling[31], we
129 hypothesize that loop 7 is a central component of the physiological switch.

130 To explore the structural changes promoted by c-di-GMP via loop 7 we tried to crystallize the apo form
131 of SmbA protein as well as SmbA$_{R211A}$ and a SmbA$_{\Delta loop}$ mutant with partial loop deletion (fragment
132 198-215 deleted) in complex with c-di-GMP. We only obtained suitable crystals for SmbA$_{\Delta loop}$(
133 Supplementary Fig. S1a), which diffracted extremely well to 1.4 Å resolution and belong to space group
134 P4$_3$2$_1$2 with one molecule in the asymmetric unit. The structure was determined by molecular
135 replacement using the structure of wild-type SmbA (PDB: 6GS8[31]) after removing c-di-GMP from the
136 model as a template, followed by iterative refinement. The data collection and refinement statistics are
137 summarized in Table 1.

138 The crystal structure shows that SmbA$_{\Delta loop}$ forms a crystallographic dimer stabilized by a monomeric
139 c-di-GMP molecule (Fig. 2a). The ligand is found in a fully extended conformation and makes isologous
140 interactions with the two protomers of the protein dimer (Fig. 2b). The guanine bases of c-di-GMP
141 interact extensively, via both polar and nonpolar contacts, with monomers A and B of the dimer. As in
142 the wild-type complex, they form cation–π interactions with the guanidinium groups of R143 from both
143 protomers (Fig. 2b). Detailed interactions will be discussed in detail further below.

144 In solution, the c-di-GMP to-protein stoichiometry using ITC was 1:1 (Supplementary Fig. S1b) and
145 not 1:2 as would have been expected from the crystal structure, indication that SmbA$_{\Delta loop}$ dimer
146 formation occurs probably only at very high concentration as used for crystallization or during crystal
147 formation.

148 In addition to the SmbA$_{\Delta loop}$/c-di-GMP complex, we also determined a crystal structure of the protein
149 in the absence of c-di-GMP. Overall, apo SmbA$_{\Delta loop}$ shows virtually the same structure as in complex
150 with c-di-GMP with an rmsd value of 0.49 Å for 225 Cα atoms (Fig. 3d). The Crystal contains four
151 molecules in the asymmetric unit. Given the relatively small interface and loose packing in the crystal
152 lattice, we consider the inter-molecular interactions to be crystallographic artifacts (Fig. 2c).

153 As measured directly by sedimentation velocity analytical ultracentrifugation (AUC-SV), apo SmbA$_{\Delta loop}$
154 is monomeric with a sedimentation coefficient of 1.73 s (Fig. 4). Addition of c-di-GMP does not change
155 the sedimentation coefficient significantly. In addition, a small secondary peak is generated at 2.3 S,
156 which may indicate some dimer formation. In contrast, SmbA$_{wt}$ experiences a substantial shift in the
157 sedimentation coefficient upon c-di-GMP addition, probably due to the larger mass of the dimeric
158 ligand and the induced change in protein shape due to loop 7 ordering. As shown in Fig. 4b, a single
159 species was observed in all cases with estimated masses were about 38 and 32 kDa for SmbA$_{wt}$ and

160 SmbA$_{\Delta loop}$, respectively. No significant difference in S and f/f$_0$ upon addition of c-di-GMP was observed

161 for both proteins (Fig. 4b). This result is consistent with our previous report that SmbA$_{wt}$ does not change

162 its oligomeric state upon c-di-GMP binding as derived from MALS data[31]. These results further support

163 that, in solution a single c-di-GMP molecule does not cause SmbA$_{\Delta loop}$ to dimerization.

164 C-di-GMP-mediated dimer stabilization has been observed previously, involving dimeric, and

165 tetrameric c-di-GMP in the case of VpsT[32] and BldD[19], respectively (for a review see ref. 27).

166 Furthermore, c-di-GMP accommodation in the rigid dimer interface has been described for STING

167 protein[33]. Notably, structure comparison shows that VpsT, STING, and SmbA involve symmetric

168 stacking interactions (with W131, Tyr167, and R143, respectively) which cap two guanine bases of c-

169 di-GMP from both sides at the dimer interface (Supplementary Fig. S2). We anticipate that protein

170 dimerization involved c-di-GMP with isologous interactions may be operational in more, hitherto

171 unrecognized target

172 **Apo and c-di-GMP bound SmbA$_{\Delta loop}$ structures and comparison with SmbA$_{wt}$ structures**

173 Overall, the SmbA$_{\Delta loop}$ mutant retains the TIM-barrel fold with eight α-helices on the outside and eight

174 parallel β-strands on the inside with an extra helix 9 (Fig. 3a). The occupancy of the c-di-GMP ligand

175 was set to 50% to account for its binding across the crystallographic dyad (half of the c-di-GMP

176 molecule belongs to the symmetry mate). The ligand fit to the electron density very well after

177 considerable conformational adjustment of both guanine bases (Fig. 3b and supplementary Fig. S3).

178 Thus, the mutant can accommodate only monomeric c-di-GMP, likely due to the absence of R211 and

179 D214 of the RxxD motif of loop 7 essential for c-di-GMP dimer coordination (Fig. 3b). As discussed

180 in the previous section, the monomeric c-di-GMP ligand forms isologous interaction with the two

181 protomers of the dimer (Fig. 2). The interactions of each guanyl with the protein are the same as

182 observed for the proximal guanyl moiety (G4) of dimeric c-di-GMP and G of ppGpp interacting with

183 wild-type SmbA[31] (Fig. 3c). R143 is found stacked upon the guanyl to form a cation–π interaction, R78

184 forms an H-bond with O6, and E188 forms on H-bond with N1 of the guanyl base (Figs. 3b and

185 supplementary S3). Compared to the wild-type complex the phosphate has moved towards the protein

186 and forms an H-bond with main-chain amide 80 (Fig. 3c). Three well-defined water molecules make

187 hydrogen bonds with R78, E188, and R143 (Fig. 3c).

188 Structural superimposition of SmbA$_{\Delta loop}$/c-di-GMP with SmbA$_{wt}$/(c-di-GMP)$_2$ (6GS8) and

189 SmbA$_{wt}$/ppGpp (6GTM) shows RMS deviations of SmbA$_{\Delta loop}$/c-di-GMP of 0.39 Å (for 214 Cα atoms)

190 and 0.46 Å (for 230 Cα atoms) when compared to SmbA$_{wt}$/c-di-GMP (Fig. 5b) and SmbA/ppGpp,

191 respectively (Fig. 5b). These values indicate virtually idendical structures, but there are some notable

192 local deviations. Particularly, in the SmbA$_{\Delta loop}$/c-di-GMP complex, the C-terminal part of loop 7 forms

193 a short helix α7* (Fig. 5a). In addition, significant changes are observed in the C-terminal helix 9,

194 which, in the wild-type protein, is stabilized by loop 7 being in turn immobilized by dimeric c-di-GMP.

195 Thereby, the G1 and G2 guanyl bases interact with the RxxD motif of loop 7[31]. In the SmbA$_{\Delta loop}$/c-di-

196 GMP complex, the monomeric ligand adopts an outward-open conformation similar to that found in

197 SmbA$_{WT}$/ppGpp complex (Fig. 4b). However, its guanyl is in the same position as the G of ppGpp and

198 G4 of c-di-GMP all forming interactions with R78 and R143 (Figs. 3c and 5). At the same time, the

199 phosphate moieties of monomeric c-di-GMP bound to SmbA$_{\Delta loop}$ do not superimpose with those of

200 bound dimeric c-di-GMP or ppGpp as bound to wild-type SmbA (Fig. 3c).

201 Because the the apo structure of SmbA$_{wt}$ is not known, we turned to a model of apo wild-type SmbA
202 generated by AlphaFold2[34] (AF2) as deposited in Uniprot (Q9A5E6) to predict the protein conformation
203 and more specifically loop 7 in an unliganded state. The AF2 model of SmbA$_{wt}$ agrees very well with
204 our X-ray structure (Fig. 5d). Indeed, the core of the TIM-barrel fold shows very high confidence
205 (pLDDT > 90) and represents the most stable region of the SmbA structure. Interestingly, loop 7 and
206 helix 9 have low (70 > pLDDT > 50) and very low (pLDDT <50) scores. It has been shown that AF2
207 correlated with the root mean square fluctuations (RMSF) calculated from MD (Molecular Dynamics)
208 simulations experiments[35]. Thus the low AF2 scores of SmbA$_{wt}$, suggest flexibility of loop 7 in the
209 absence of c-di-GMP (Supplementary Fig. S 5a) which is most likely is open in the unliganded state in
210 contrast to closed in SmbA$_{wt}$/(c-di-GMP)$_2$ structure (Figs. 5c and 5d). This prediction is in line with
211 the functional model of SmbA action[31] which posits that, in response to c-di-GMP binding, the protein
212 switches form an on- to off on-state accompanied by structural changes in flexible loop 7 and helix 9,
213 which ultimately controls the interaction with an unknown downstream partner possibly via
214 heterodimerization (Supplementary Fig. S 5b).

Conformation of the monomeric c-di-GMP bound to SmbA$_{\Delta loop}$

216 As discussed above, with the deletion of the loop containing the RxxD motif SmbA loses its ability to
217 bind intercalated dimeric c-di-GMP molecule but still can hold one c-di-GMP. The monomeric ligand
218 is two-fold symmetric, where the sugar pucker is C3′-endo, and both glycosidic torsion angles have a
219 value of -126° (Figs. 6a and 6b), which is significantly distinct to the *trans* conformation of G4 as part
220 of dimeric c-di-GMP bound to wild-type SmbA. Superposition of c-di-GMP from the SmbA$_{\Delta loop}$ and
221 SmbA$_{wt}$ complex structures shows that this difference is the reason for the elongated shape of
222 monomeric c-di-GMP, while macrocycle including the sugar superimposes closely (Fig. 6c).

223 Next, we compared the conformation of monomeric c-di-GMP as bound to SmbA$_{\Delta loop}$ to other effectors
224 that bind the ligand in the monomeric form such as the phosphodiesterase domain PdeL$_{EAL}$[36] and the
225 degenerate LapD$_{EAL}$ domain[37]. A superposition of the three complexes is shown in Fig. 6d. While the
226 macrocycles retain a similar, but not identical, conformation, as seen in the SmbA$_{\Delta loop}$, the ligands bound
227 to PdeL$_{EAL}$ and LapD$_{EAL,}$ are in a more open conformation, apparently due to the C2′-endo puckering of
228 one of the guanines (at the right side in Fig. 6d). These results show that c-di-GMP can adopt yet another
229 unique conformation different from the stacked dimeric conformation in complex with SmbA$_{wt}$, or the
230 extended form in the PdeL$_{EAL}$ (PDB code-4LJ3) or degenerate LapD$_{EAL}$ domain (PDB code-3PJT).

231 The monomeric c-di-GMP conformation observed in the SmbA$_{\Delta loop}$ complex structure is different from
232 that of dimeric c-di-GMP. From this comparison, one can see that one G1 is bound always the same
233 way in the three complexes (Fig. 3c). Due to the conformational changes, the other GMP has moved
234 out considerably, to form an isologous interaction with the second SmbA$_{\Delta loop}$ molecule (interacting
235 residues from monomer B is not shown) (Fig. 3c). This indicates that, depending on its binding partner,
236 c-di-GMP is flexible enough to adopt various conformations via only minor changes in torsion-angle.

The SmbA$_{\Delta loop}$/c-di-GMP structure may represent the first step of consecutive c-di-GMP binding to form an intercalated dimer

239 At very high (>1 mM) concentration, c-di-GMP can form dimers or even higher oligomers, such as
240 tetramers or octamers. However, Gentner et al. (2012) clearly showed by NMR that c-di-GMP is

241 monomeric at physiological concentrations[38]. However it cannot be ruled out, but is unlikely, that other
242 factors (metal ions, molecular crowding and aromatic compounds) may favor higher oligomers in the
243 cellular environment. Intercalated c-di-GMP dimers have been observed in several protein complexes,
244 such as when bound to the I-site of diguanylate cyclases, or in response regulators, PilZ receptors, and
245 SmbA$_{wt}$. Based on our data shown here, we propose that at physiological concentrations c-di-GMP
246 dimerization occurs only on the protein by consecutive binding of c-di-GMP monomers to form the
247 intercalated dimer (Fig. 6e).

248 This obviously implies the presence of a well formed, high-affinity protein binding site for the first c-
249 di-GMP molecule. Here, we have captured upon loop deletion for the first time a potential binding pose
250 of the first c-di-GMP binding event to SmbA. Indeed, all interactions required to bind this first monomer
251 (involving R143, E188, R78) are present in SmbA$_{\Delta loop}$ (Fig. 3c) and the affinity turned out to be in the
252 low μM range (Fig. S1b). For the second binding event, in addition to a bound c-di-GMP molecule
253 providing guanyl stacking sites, loop 7 providing the R$_{211}$xxD$_{214}$ motif would then be required
254 (Supplementary Fig. S1e). In line with the structural considerations, the affinity of c-di-GMP to
255 SmbA$_{\Delta loop}$ is in the low micromolar range and is in fact comparable to the apparent K$_d$ of c-di-GMP to
256 the wild-type protein (Supplementary Fig. S1 c and d).

257 In line with the structural considerations and the proposed binding mechanism, the K$_d$ of c-di-GMP to
258 SmbA$_{\Delta loop}$ is low (1.8 μM) (Fig. S1b) and, in fact comparable, to the apparent K$_d$ (0.3 μM) of the
259 compound to the wild-type protein (Fig. S1c). For completeness, the affinity of ppGpp to the SmbA
260 mutant was also measured (Fig. S1d) and was found to be virtually identical to the affinity of the
261 compound to SmbA$_{w31t}$ indicating that loop 7, as expected, does not contribute to ppGpp binding. In
262 summary, the hypothesis of consecutive c-di-GMP binding to form an intercalated dimer on the protein
263 is strongly supported by the results on the SmbA loop deletion mutant.

Phylogenetic analysis and exploring SmbA homologs

265 To understand the evolutionary significance of the flexible loop of SmbA switch protein, here we have
266 further extended our primary sequence analysis of SmbA and its homologs described briefly in Shyp et
267 al. 2021. We identified SmbA orthologs based on reciprocal best BLAST hits across species,
268 concordance of the protein sequence distance tree with a species phylogeny based on 16S rRNA
269 markers[39] and syntenic conservation[40] (Figs. 7a and 7b). Interestingly, the c-di-GMP-binding RxxD
270 motif is only strictly conserved within the *Caulobacter* genus, with either Asn or Glu substitution
271 among the *Caulobacterales* (Fig. 7c). There is considerable variability around this loop region,
272 including several insertions and deletion events. This may suggest alternative binding modes and/or
273 substrates within the *Caulobacterales* order. Similarly, the sites interacting with ppGpp (R78, N111,
274 Q114, R143, E188) are not strictly conserved within the *Caulobacterales* order. The C-terminal helix
275 9 is highly conserved among SmbA orthologs (Fig. 7c). This is consistent with the proposal that it
276 adopts a different conformation in the c-di-GMP-bound state than apo and ppGpp, thus necessary for
277 the ligand-mediated SmbA switch. A similar mechanism may apply to other SmbA orthologs via
278 interplay of unknown ligands. The strictly conserved N-terminal motif (MRYRP[FL]G) is also found
279 in otherwise unrelated proteins from the *Acetomycetalesorder* (Frankia, Streptomyces).

280 The *Caulobacterales* order contains prosthecate and non-prosthecate species[39,41]. SmbA (Q9A5E6)
281 appears to be unique to the prosthecate *Caulobacterales*. Reciprocal best BLAST hits for SmbA from

282 non-prosthecate *Caulobacterales* and other bacterial species are very distantly related Aldo-keto
283 reductases which cannot be meaningfully aligned with SmbA. The central function of SmbA is a simple
284 molecular switch that responds to the cellular concentrations of ppGpp and c-di-GMP to regulate
285 *Caulobacter* growth [31]. We surmise that the presence of a SmbA ortholog is a marker for prosthecate-
286 type *Caulobacterales* species which have not been morphologically characterized. This is further
287 supported by the genes flanking SmbA, including a putative iron-sulfur glutaredoxin (Q9A5E5) and a
288 BolA/YrbA family transcription factor (Q9A5E7) which in *E. coli* positively regulates the transition
289 from the planktonic to attachment stage of biofilm formation[42].
290

Material and methods

292

Plasmid construction and purification of the recombinant protein

294 To construct pET21b-smbA$_{\Delta loop}$-His6 (deletion of fragment 198-215), the pET21b-smbA-His6 plasmid
295 was amplified with the following primers: 6265_D Loop7_forward
296 CCCCAGGCCCTGCGAGAACTGGCCGATGTGGGCGGCTA and 6266_DLoop7_reverse
297 TAGCCGCCCACATCGGCCAGTTCTCGCAGGGCCTGGGG. The template was digested with
298 DpnI and mutant DNA was transformed into competent cells for nick repair. The final construct has
299 been sequenced to confirm the fragment deletion. Protein was overproduced and purified as described
300 previously[31]. *E. coli* Rosetta 2(DE3) cells were used to overproduce recombinant protein from the
301 pET21b expression plasmid. Cells were grown in LB-Miller supplemented with 100 μg/ml ampicillin
302 to an OD$_{600}$ of 0.4 to 0.6, expression was induced with 1 mM IPTG overnight at 22°C. Cells were
303 harvested by centrifugation (5000 g, 20 min, 4°C), washed with PBS and flash-frozen in liquid N$_2$, and
304 stored at -80°C until purification.

305 For purification, cells were resuspended in *lysis buffer* (30 mM Tris/HCl pH 7.5, 5 mM MgCl$_2$, 100
306 mM NaCl, 1mM DTT and 10 mM imidazole containing 0.2 mg/ml lysozyme, DNaseI (AppliChem)
307 and Complete Protease inhibitor (Roche) and disrupted using a French press. The suspension was
308 clarified by centrifugation at 30,000 x g (Sorval SLA 1500) at 4 °C for 30 min and loaded onto a 1 ml
309 HisTrap HP column (GE Healthcare) on an ÄKTA purifier 10 system (GE Healthcare). Column was
310 washed with 5 column volumes with *wash buffer* (30 mM Tris/HCl pH 7.5, 5 mM MgCl$_2$, 100 mM
311 NaCl, 1mM DTT and 10 mM imidazole), and the bound protein was eluted with linear gradient of
312 *elution buffer* (30 mM Tris/HCl pH 7.5, 3mM MgCl$_2$, 100 mM NaCl, 1mM DTT and 300 mM
313 imidazole). Elution fractions enriched in SmbA (as judged by SDS-PAGE) were pooled and
314 concentrated to around 10 mg/ml using Amicon Ultra centrifugal concentrator with a nominal molecular
315 weight cut-off of 30 kDa (Millipore AG). The concentrated protein was centrifuged at 16,000 x g at
316 4°C for 15 min and loaded onto a Superdex 75 gel filtration column (Amersham Biosciences)
317 equilibrated with 30 mM Tris/HCl pH 7.5, 5 mM MgCl$_2$, 100 mM NaCl, 1mM DTT. Fractions
318 containing essentially pure SmbA (as judged by SDS-PAGE) were pooled and concentrated to a desired
319 concertation for further experiments.

Crystallization

321 A Phoenix robot (Art Robbins Instruments) was used for a wide range of crystallization screening.
322 Crystallization was carried out using the sitting drop vapour diffusion method at 20 °C by mixing the

protein with the reservoir solution in a 1:1 ratio. The protein concentration was 5.0, 2.25 and 1.75 mg/ml upon adding c-di-GMP in 3.0 fold molar excess. Triangle diamond-shaped 3D crystals appeared in Pact premier D11 (Molecular dimension) after one week in 0.2 M Calcium chloride dihydrate 0.1 M Tris pH 8.0 and 20 % w/v PEG 6000. Crystals were flash-frozen into two different cryoprotectants. The best diffraction was obtained from crystals cryo-protected with 25% ethylene glycol.

For the apo protein crystals, three different protein concentrations (20, 15 and 5 mg/ml) were used at room temperature. Crystals appeared within a week and continued growoing for a few additional days in a condition containing 200 mM NaCl and 10 % v/w PEG 6000. The crystals were flash-frozen in liquid N2 for data collection at 100 K.

X-Ray diffraction data collection, phasing, and refinement

All single-crystal X-ray diffraction data sets were collected at PXI and PXIII beamline of Swiss Light source, Villigen, Switzerland.) Datasets were collected for the crystal of the SmbAΔloop apo and in presence of c-di-GMP. Diffraction data sets were processed either with MOSFLM[43] or XDS[44] and the resulting intensities were scaled using SCALA from CCP4/CCP4i2 suite[45]For solving the SmbA$_{\Delta loop}$ apo and complex structure, SmbA$_{wt}$ (PDB code, 6GS8) structure was used as search model without c-di-GMP. Both structures were solved by molecular replacement using PHENIX PHASER[46]. Further refinement of structures was carried out using REFMAC5 and Phenix refinement[47]. Model building was performed using COOT[48] and model validation was carried out with molprobity[49]. Crystallographic data processing and refinement statistics are provided in Table 1.

Isothermal titration calorimetry (ITC)

Experiments were carried out at 25°C or 10°C, a syringe stirring speed of 300 rpm, a pre-injection delay of 200 secs, and a recording interval of 250 secs in a Microcal VP-ITC in ITC buffer (30 mM Tris-HCl pH 7.5, 150 mM NaCl, 5 mM MgCl$_2$). All solutions were degassed below the temperature used in the experiments before loading into the calorimeter cell. Baseline correction and integration of the raw differential power data, and fitting of the resulting binding isotherms to obtain dissociation constants were performed using the Microcal ORIGIN software.

Analytical ultracentrifugation (AUC)

Sedimentation velocity (SV) centrifugation was performed on a ProteomLab™ XL-A analytical ultracentrifuge (Beckman-Coulter, Brea, CA, USA) using an AN60 Ti rotor with standard aluminum 2-channel centerpieces with quartz windows. The samples were spun at speeds ranging from 35000 to 50000 rpm depending on the protein size at 4°C. The SmbA$_{wt}$ (38.9 μM) and SmbA$_{\Delta loop}$ (39.0 μM) in SEC buffer was subjected to ultracentrifugation in the absence and in presence of a 5 fold molar excess of c-di-GMP. Radial scans were recorded with 30 μm radial resolution at ~3 min intervals. The software packages SEDFIT v 14.14 was used for data evaluation. After transformation of the recorded sedimentation velocity data taken in the intensity mode to interference data in the respective data evaluation software, time- as well as radially-invariant noise were calculated and subtracted. In SEDFIT (http://www.analyticalultracentrifugation.com), continuous sedimentation coefficient distributions c(s) were determined with 0.05 S resolution and an F-ratio = 0.95. Suitable s-value ranges between 0 and 30 S and for GA f/f$_0$ between 1 and 4 were chosen. Buffer density (1.0136 g/ml) and viscosity (1.591 cP) were calculated with SEDNTERP v 20111201 beta (http://bitcwiki.sr.unh.edu/index.php). The

partial specific volumes of the studied proteins were calculated according to the method of Cohn and Edsall as implemented in SEDNTERP. From the peak in the c(s) distribution, the frictional ratio f/f0 and the meolecular weight were obtained by SEDFIT based on the Stokes-Einstein and Svedberg equations[50] (REF. Braun and Schuck 2006). Data were plotted using program ProFit (Quansoft, Zurich, Switzerland).

AlphaFold modeling

The SmbAwt AphaFold model was retrieved from Uniprot (https://www.uniprot.org) with accession code Q9A5E6. The X-ray structures were visualized using Pymol (https://pymol.org/2/) and compared to the AlphaFold model.

Bioinformatics

BLAST analyses were conducted using the NCBI-NR dataset. Multiple sequence alignments were generated using MAFFT in G-INS-i mode[51] followed by manual refinement. The phylogenetic tree of 24 SmbA orthologs was inferred using the Maximum Likelihood method based on the JTT model[52] as implemented in MEGA7[53]. Branch lengths indicate the number of substitutions per site. The tree with the highest log likelihood (-9134.38) is shown, with bootstrap support from 100 replicates indicated at branches. Initial tree(s) for the heuristic search were obtained automatically by applying Neighbor-Join and BioNJ algorithms to a matrix of pairwise distances estimated using a JTT model, and then selecting the topology with a superior log-likelihood value. A discrete Gamma distribution was used to model evolutionary rate differences among sites (5 categories, +G = 2.2328)). The rate variation model allowed for some sites to be evolutionarily invariable ([+I], 7.16% sites). The tree is drawn to scale, with branch lengths measured in the number of substitutions per site. There were a total of 323 positions in the final dataset.

Data availability

The final SmbA$_{\Delta loop}$ coordinates and structure factor amplitudes have been deposited in the Protein Data Bank (PDB) and are available under accession number 7B0E (SmbA$_{\Delta loop}$/c-di-GMP) and 8BVB (SmbA$_{\Delta loop}$).

References

413

1. Hauryliuk, V., Atkinson, G. C., Murakami, K. S., Tenson, T. & Gerdes, K. Recent functional insights into the role of (p)ppGpp in bacterial physiology. *Nat Rev Microbiol* 13, 298–309 (2015).

2. Jenal, U., Reinders, A. & Lori, C. Cyclic di-GMP: second messenger extraordinaire. *Nat Rev Microbiol* 15, 271–284 (2017).

3. Cashel, M. & Gallant, J. Two compounds implicated in the function of the RC gene of Escherichia coli. *Nature* 221, 838–41 (1969).

4. Dalebroux, Z. D. & Swanson, M. S. ppGpp: magic beyond RNA polymerase. *Nat Rev Microbiol* 10, 203–212 (2012).

5. Kalia, D. *et al.* Nucleotide, c-di-GMP, c-di-AMP, cGMP, cAMP, (p)ppGpp signaling in bacteria and implications in pathogenesis. *Chem Soc Rev* 42, 305–341 (2012).

6. Potrykus, K., Murphy, H., Philippe, N. & Cashel, M. ppGpp is the major source of growth rate control in E. coli. *Environ Microbiol* 13, 563–575 (2011).

7. Stott, K. V. *et al.* (p)ppGpp modulates cell size and the initiation of DNA replication in Caulobacter crescentus in response to a block in lipid biosynthesis. *Microbiology+* 161, 553–564 (2015).

8. Wood, A., Irving, S., Bennison, D. & Corrigan, R. The (p)ppGpp-binding GTPase Era promotes rRNA processing and cold adaptation in Staphylococcus aureus. *Access Microbiol* 2, (2020).

9. Gonzalez, D. & Collier, J. Effects of (p)ppGpp on the Progression of the Cell Cycle of Caulobacter crescentus. *J Bacteriol* 196, 2514–2525 (2014).

10. Lesley, J. A. & Shapiro, L. SpoT Regulates DnaA Stability and Initiation of DNA Replication in Carbon-Starved Caulobacter crescentus. *J Bacteriol* 190, 6867–6880 (2008).

11. Martins, D. *et al.* Superoxide dismutase activity confers (p)ppGpp-mediated antibiotic tolerance to stationary-phase Pseudomonas aeruginosa. *P Natl Acad Sci Usa* 115, 9797–9802 (2018).

12. Nguyen, D. *et al.* Active Starvation Responses Mediate Antibiotic Tolerance in Biofilms and Nutrient-Limited Bacteria. *Science* 334, 982–986 (2011).

442   13. Boehm, A. *et al.* Second Messenger-Mediated Adjustment of Bacterial Swimming
443   Velocity. *Cell* 141, 107–116 (2010).

444   14. Matsuyama, B. Y. *et al.* Mechanistic insights into c-di-GMP–dependent control of the
445   biofilm regulator FleQ from Pseudomonas aeruginosa. *Proc National Acad Sci* 113, E209–
446   E218 (2016).

447   15. Baraquet, C. & Harwood, C. S. Cyclic diguanosine monophosphate represses bacterial
448   flagella synthesis by interacting with the Walker A motif of the enhancer-binding protein
449   FleQ. *Proc National Acad Sci* 110, 18478–18483 (2013).

450   16. Fazli, M. *et al.* Regulation of biofilm formation in Pseudomonas and Burkholderia
451   species. *Environ Microbiol* 16, 1961–1981 (2014).

452   17. Morgan, J. L. W., McNamara, J. T. & Zimmer, J. Mechanism of activation of bacterial
453   cellulose synthase by cyclic-di-GMP. *Nat Struct Mol Biol* 21, 489–496 (2014).

454   18. Römling, U., Gomelsky, M. & Galperin, M. Y. C-di-GMP: the dawning of a novel
455   bacterial signalling system. *Mol Microbiol* 57, 629–639 (2005).

456   19. Tschowri, N. *et al.* Tetrameric c-di-GMP Mediates Effective Transcription Factor
457   Dimerization to Control Streptomyces Development. *Cell* 158, 1136–1147 (2014).

458   20. Lori, C. *et al.* Cyclic di-GMP acts as a cell cycle oscillator to drive chromosome
459   replication. *Nature* 523, 236–239 (2015).

460   21. Dubey, B. N. *et al.* Cyclic di-GMP mediates a histidine kinase/phosphatase switch by
461   noncovalent domain cross-linking. *Sci Adv* 2, e1600823 (2016).

462   22. Dubey, B. N. *et al.* Hybrid histidine kinase activation by cyclic di-GMP–mediated
463   domain liberation. *Proc National Acad Sci* 117, 1000–1008 (2020).

464   23. Li, X., Chen, F., Xiao, J. & He, J. [Structure and function of c-di-GMP riboswitches].
465   *Sheng Wu Gong Cheng Xue Bao Chin J Biotechnology* 33, 1357–1368 (2017).

466   24. Leduc, J. L. & Roberts, G. P. Cyclic di-GMP Allosterically Inhibits the CRP-Like Protein
467   (Clp) of Xanthomonas axonopodis pv. citri. *J Bacteriol* 191, 7121–7122 (2009).

468   25. Krasteva, P. V. & Sondermann, H. Versatile modes of cellular regulation via cyclic
469   dinucleotides. *Nat Chem Biol* 13, 350–359 (2017).

470   26. Hengge, R. Principles of c-di-GMP signalling in bacteria. *Nat Rev Microbiol* 7, 263–273
471   (2009).

472   27. Chou, S.-H. & Galperin, M. Y. Diversity of Cyclic Di-GMP-Binding Proteins and
473   Mechanisms. *J Bacteriol* 198, 32–46 (2016).

474   28. Wang, Y.-C. *et al.* Nucleotide binding by the widespread high-affinity cyclic di-GMP
475   receptor MshEN domain. *Nat Commun* 7, 12481 (2016).

476 29. Nesper, J., Reinders, A., Glatter, T., Schmidt, A. & Jenal, U. A novel capture compound
477 for the identification and analysis of cyclic di-GMP binding proteins. *J Proteomics* 75, 4874–
478 4878 (2012).

479 30. Haas, T. M. *et al.* Photoaffinity Capture Compounds to Profile the Magic Spot Nucleotide
480 Interactomes**. *Angew. Chem. Int. Ed.* 61, e202201731 (2022).

481 31. Shyp, V. *et al.* Reciprocal growth control by competitive binding of nucleotide second
482 messengers to a metabolic switch in Caulobacter crescentus. *Nat Microbiol* 6, 59–72 (2021).

483 32. Krasteva, P. V. *et al.* Vibrio cholerae VpsT regulates matrix production and motility by
484 directly sensing cyclic di-GMP. *Sci New York N Y* 327, 866–8 (2010).

485 33. Shang, G. *et al.* Crystal structures of STING protein reveal basis for recognition of cyclic
486 di-GMP. *Nat Struct Mol Biol* 19, 725–7 (2012).

487 34. Jumper, J. *et al.* Highly accurate protein structure prediction with AlphaFold. *Nature* 596,
488 583–589 (2021).

489 35. Guo, H.-B. *et al.* AlphaFold2 models indicate that protein sequence determines both
490 structure and dynamics. *Sci Rep-uk* 12, 10696 (2022).

491 36. Sundriyal, A. *et al.* Inherent Regulation of EAL Domain-catalyzed Hydrolysis of Second
492 Messenger Cyclic di-GMP*. *J Biol Chem* 289, 6978–6990 (2014).

493 37. Navarro, M. V. A. S. *et al.* Structural Basis for c-di-GMP-Mediated Inside-Out Signaling
494 Controlling Periplasmic Proteolysis. *Plos Biol* 9, e1000588 (2011).

495 38. Gentner, M., Allan, M. G., Zaehringer, F., Schirmer, T. & Grzesiek, S. Oligomer
496 Formation of the Bacterial Second Messenger c-di-GMP: Reaction Rates and Equilibrium
497 Constants Indicate a Monomeric State at Physiological Concentrations. *J Am Chem Soc* 134,
498 1019–1029 (2012).

499 39. Abraham, W.-R. *et al.* Phylogeny by a polyphasic approach of the order Caulobacterales,
500 proposal of Caulobacter mirabilis sp. nov., Phenylobacterium haematophilum sp. nov. and
501 Phenylobacterium conjunctum sp. nov., and emendation of the genus Phenylobacterium. *Int J*
502 *Syst Evol Micr* 58, 1939–1949 (2008).

503 40. Altenhoff, A. M. *et al.* The OMA orthology database in 2015: function predictions, better
504 plant support, synteny view and other improvements. *Nucleic Acids Res* 43, D240–D249
505 (2015).

506 41. Abraham, W.-R., Rohde, M. & Bennasar, A. The Prokaryotes. 179–205 (2014)
507 doi:10.1007/978-3-642-30197-1_259.

508 42. Dressaire, C., Moreira, R. N., Barahona, S., Matos, A. P. A. de & Arraiano, C. M. BolA
509 Is a Transcriptional Switch That Turns Off Motility and Turns On Biofilm Development.
510 *Mbio* 6, e02352-14 (2015).

511   43. Leslie, A. G. W. The integration of macromolecular diffraction data. *Acta Crystallogr*
512   *Sect D Biological Crystallogr* 62, (2006).

513   44. Kabsch, W. XDS. *Acta Crystallogr Sect D Biological Crystallogr* 66, (2010).

514   45. Potterton, L. *et al.* CCP4i2: the new graphical user interface to the CCP4 program suite.
515   *Acta Crystallogr Sect D Struct Biology* 74, 68–84 (2018).

516   46. McCoy, A. J. *et al.* Phaser crystallographic software. *J Appl Crystallogr* 40, 658–674
517   (2007).

518   47. Terwilliger, T. C. *et al.* Iterative model building, structure refinement and density
519   modification with the PHENIX AutoBuild wizard. *Acta Crystallogr Sect D Biological*
520   *Crystallogr* 64, 61–69 (2008).

521   48. Emsley, P. & Cowtan, K. Coot: model-building tools for molecular graphics. *Acta*
522   *Crystallogr Sect D Biological Crystallogr* 60, 2126–2132 (2004).

523   49. Williams, C. J. *et al.* MolProbity: More and better reference data for improved all-atom
524   structure validation. *Protein Sci* 27, 293–315 (2018).

525   50. Brown, P. H. & Schuck, P. Macromolecular Size-and-Shape Distributions by
526   Sedimentation Velocity Analytical Ultracentrifugation. *Biophys J* 90, 4651–4661 (2006).

527   51. Katoh, K., Kuma, K., Toh, H. & Miyata, T. MAFFT version 5: improvement in accuracy
528   of multiple sequence alignment. *Nucleic Acids Res* 33, 511–518 (2005).

529   52. Jones, D. T., Taylor, W. R. & Thornton, J. M. The rapid generation of mutation data
530   matrices from protein sequences. *Bioinformatics* 8, 275–282 (1992).

531   53. Kumar, S., Stecher, G. & Tamura, K. MEGA7: Molecular Evolutionary Genetics
532   Analysis Version 7.0 for Bigger Datasets. *Mol Biol Evol* 33, 1870–1874 (2016).

533   54. Egli, M. *et al.* Atomic-resolution structure of the cellulose synthase regulator cyclic
534   diguanylic acid. *Proc National Acad Sci* 87, 3235–3239 (1990).

535
536
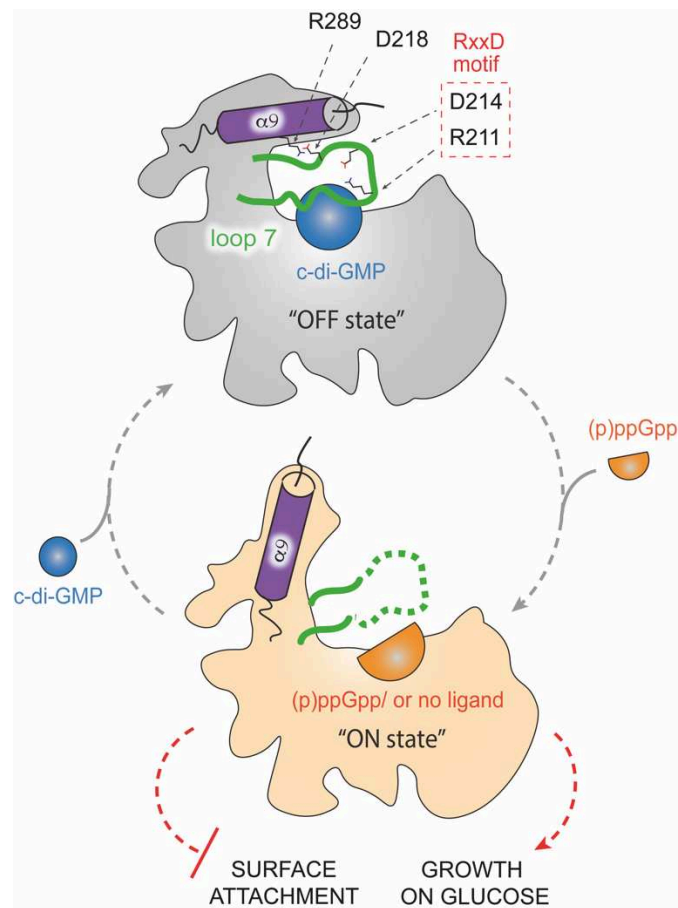537
538
539
540
541
542
543
544
545

Main Figures

Figure 1. Second messenger mediated regulation of SmbA. Binding of a c-di-GMP dimer (blue sphere) inactivates SmbA ("OFF state", grey), while its dissociation or displacement by a ppGpp monomer (an orange half-sphere) activates the protein ("ON state", light orange). Loop 7 is shown in green, the C-terminal α9 helix is represented by a magenta cylinder. Amino acid residues essential for salt bridge formation between α9 helix and loop 7 are indicated. Key residues of the RxxD motif in loop 7 are shown in the red box. The physiological functions of activated SmbA are indicated with red dashed lines (Adopted from Shyp *et al.*, 2021).
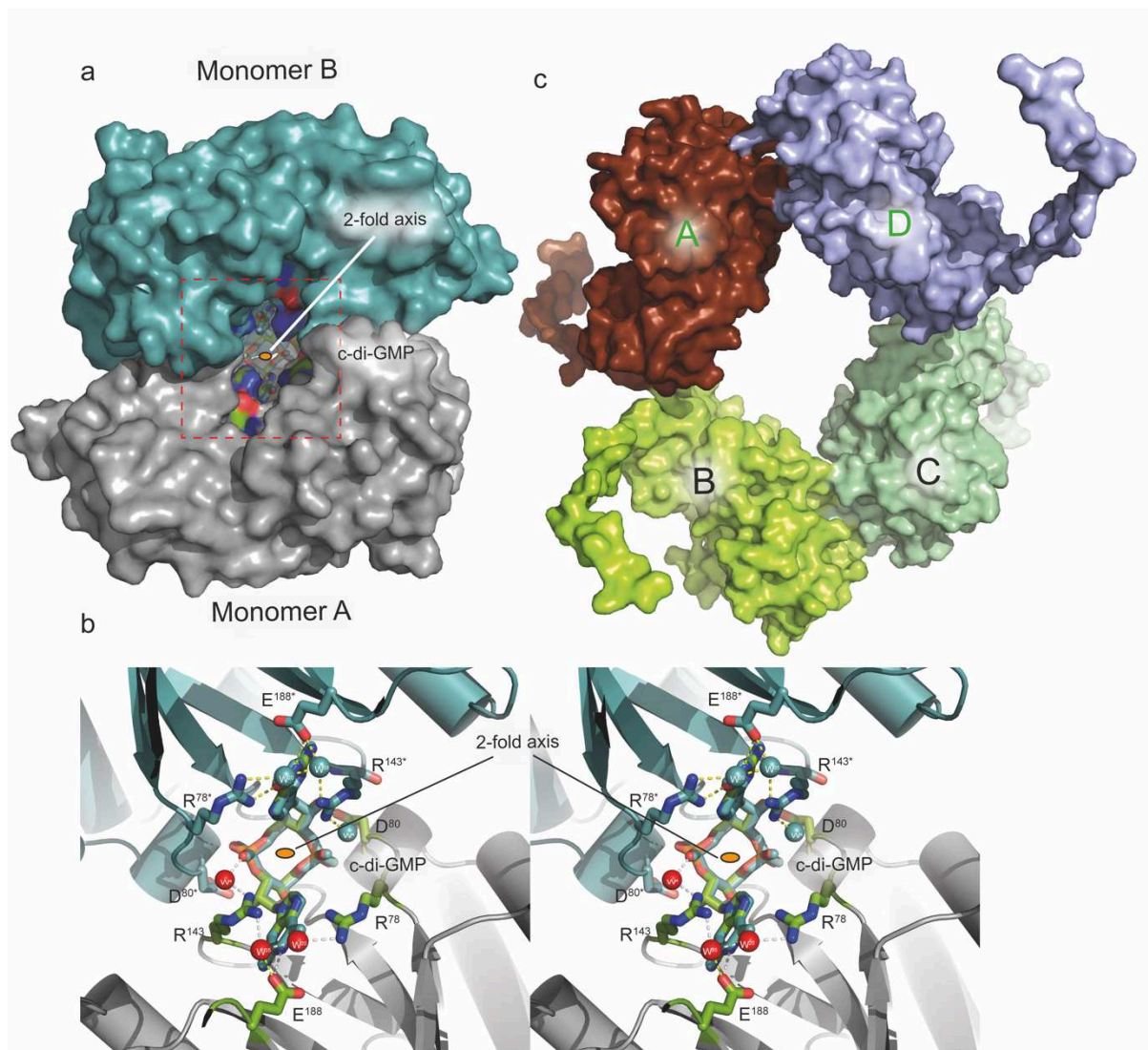
564
565

Figure 2. Crystal structures of SmbA$_{\Delta loop}$ with c-di-GMP bound across crystallographic dyad and of apo SmbA$_{\Delta loop}$. (a) The two monomers are depicted as surface (negatively charged atoms in red, positively charged atoms in blue and carbon atoms in green) with monomer A (gray) in standard orientation and monomer B (symmetry mate) in cyan. c-di-GMP (thick) in the dimer interface is shown as ball-and-stick model. **(b)** Stereoview down the twofold axis (indicated as a small orange ellipsoid), showing c-di-GMP forming isologous interactions with the two SmbA$_{\Delta loop}$ protomers. Relevant residues are shown as color-coded sticks (oxygen, red; nitrogen, blue; carbon, green or cyan and waters as red and cyan spheres) and labeled. Residues and waters of the symmetry mate monomer are marked with an asterisk. Hydrogen bonds between subunits and c-di-GMP are indicated as yellow dotted lines. **(c)** Crystal packing of apo SmbA$_{\Delta loop}$ shown in surface representation. The four molecules are arranged in an asymmetric unit form two local dimers (A and D, B and C) with 2-fold symmetry.
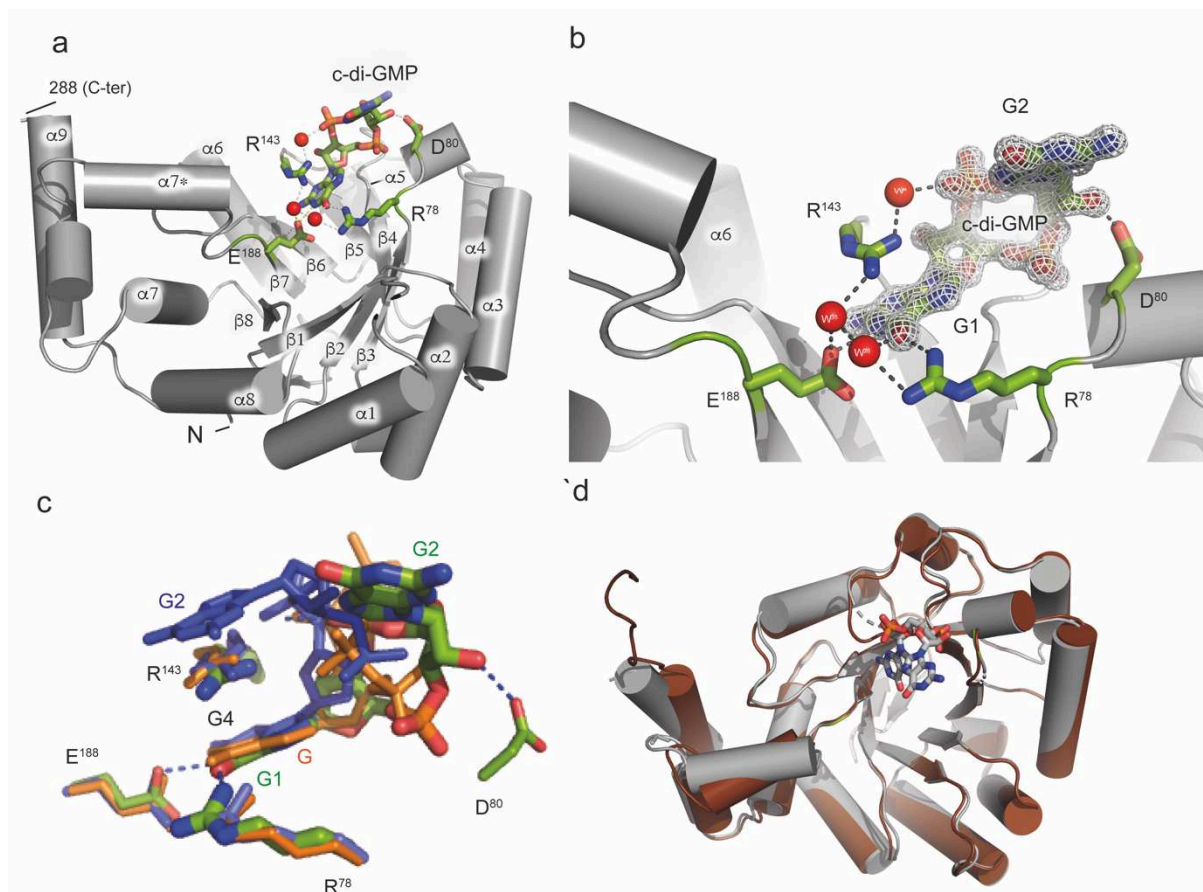
578
579
580

581

582 **Figure 3. Detailled crystal structures of SmbA$_{\Delta loop}$ in presence and absence of c-di-GMP and and**

583 **structural comparison with wild-type SmbA ligands. (a)** Crystal structure of the SmbA$_{\Delta loop}$ with

584 the backbone drawn in grey cartoon and monomeric c-di-GMP shown in a stick. Residues in

585 the SmbA$_{\Delta loop}$ important in interaction with the c-di-GMP molecule are drawn in stick

586 representation. Carbon atoms are shown in green, nitrogen in blue and oxygen in red. **(b)** 2Fo-

587 Fc omit maps contoured at 1.2 σ of c-di-GMP and full structural details of the interacting

588 residues. H-bonds (length < 3.5 Å) are indicated by gray lines and water molecules in red

589 spheres. **(c)** View of c-di-GMP (green) as bound to SmbA$_{\Delta loop}$, and the proximal c-di-GMP

590 molecule (blue) of dimeric c-di-GMP and ppGpp (orange) as bound to wild-type SmbA. The

591 proximal guanyl of monomeric c-di-GMP (G1), guanyl of ppGpp (G) and G4 of dimeric c-di-

592 GMP overlap closely. While the other guanyl (G2) of the monomeric ligand has moved out

593 considerably, to form isologous interactions with the second SmbA$_{\Delta loop}$ molecule (not shown).

594 **(d)** structural superposition of SmbA$_{\Delta loop}$/c-di-GMP (gray) with SmbA$_{\Delta loop}$ (chocolate) yielding a

595 RMSD of 0.49 Å.

596

597

598

599

600

601

a

b

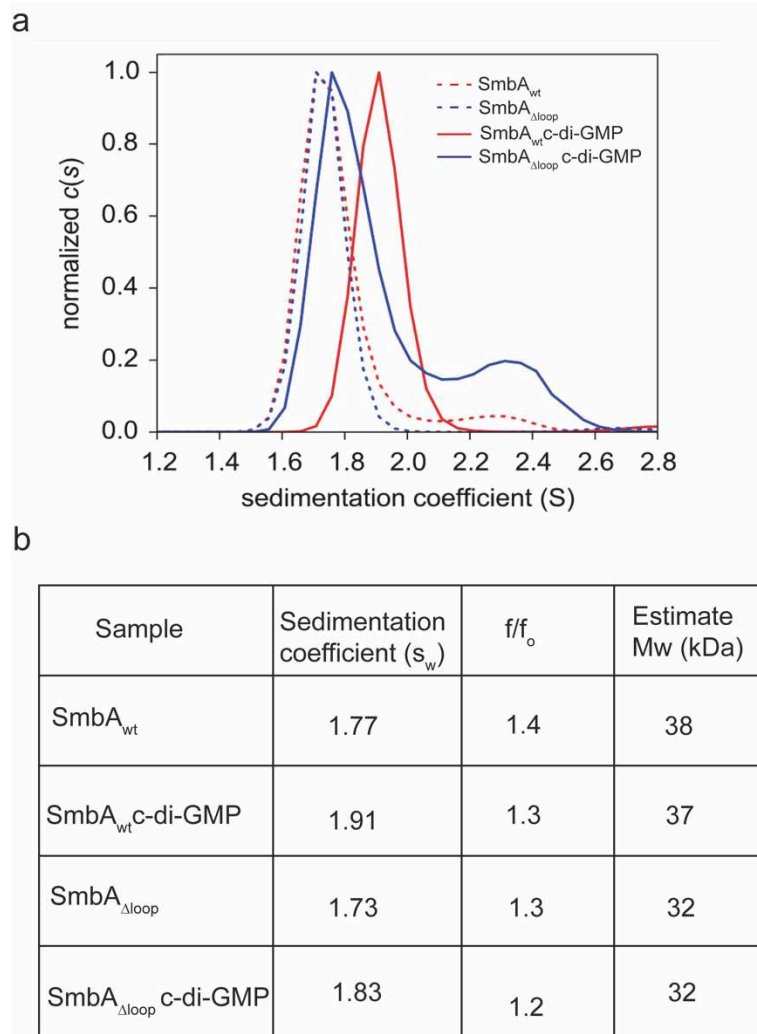| Sample	Sedimentation coefficient (s_w)	f/f_o	Estimate Mw (kDa)
SmbA$_{wt}$	1.77	1.4	38
SmbA$_{wt}$c-di-GMP	1.91	1.3	37
SmbA$_{\Delta loop}$	1.73	1.3	32
SmbA$_{\Delta loop}$ c-di-GMP	1.83	1.2	32

602
603 **Figure 4. Analytical ultracentrifugation (AUC) analysis of SmbA$_{wt}$ and SmbA$_{\Delta loop}$.**
604 **(a)** SV-AUC absorbance c(s) distributions of SmbA$_{wt}$, SmbA$_{wt}$/(c-di-GMP)$_2$, SmbA$_{\Delta loop}$ and
605 SmbA$_{\Delta loop}$/c-di-GMP. **(b)** Mass estimation and s and f/f$_O$ values of SmbA$_{wt}$, SmbA$_{wt}$/(c-di-GMP)$_2$,
606 SmbA$_{\Delta loop}$ and SmbA$_{\Delta loop}$/c-di-GMP.

607
608
609
610
611
612
613
614
615
616
617
618

619
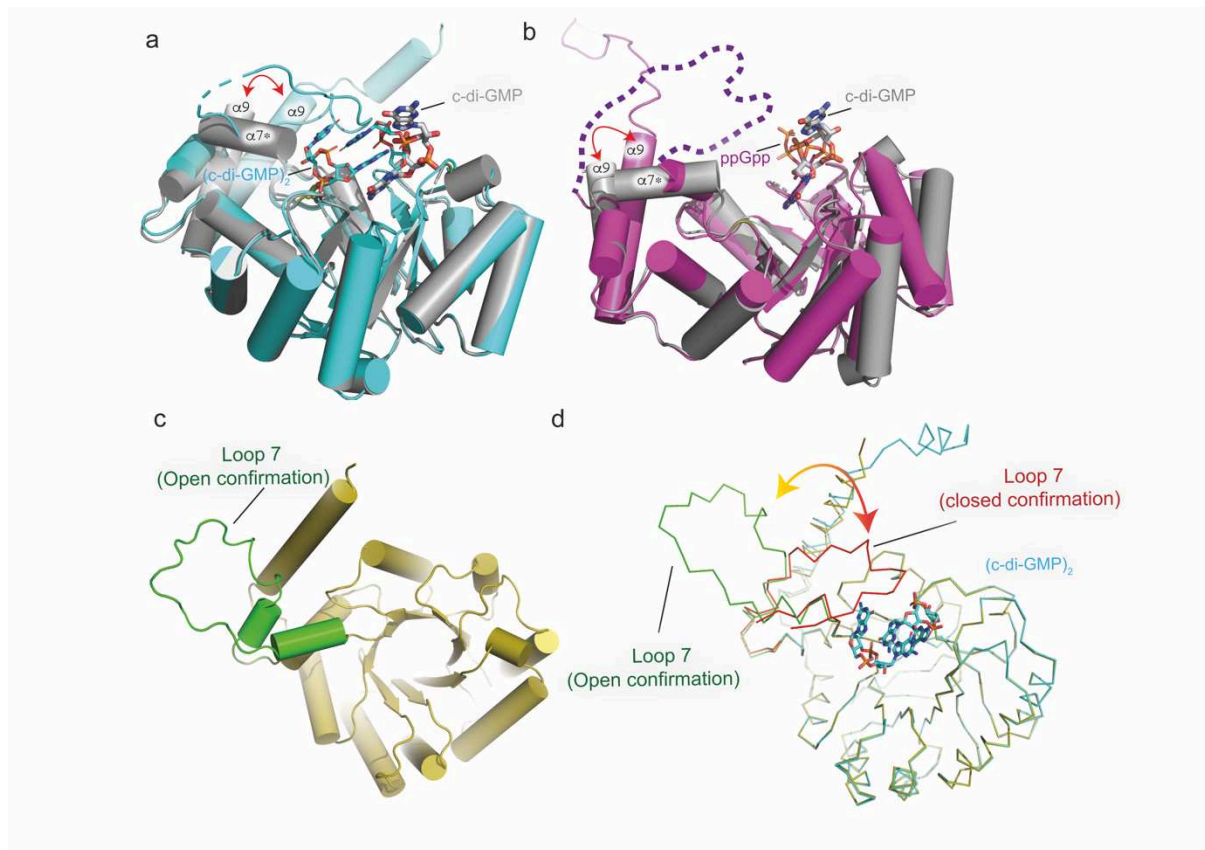
620 **Figure 5. Structural comparison of SmbA$_{\Delta loop}$/c-di-GMP with SmbA$_{wt}$/(c-di-GMP)$_2$,**

621 **SmbA$_{wt}$/ppGpp and Alphafold model of SmbA$_{wt}$. (a)** Superposition of SmbA$_{\Delta loop}$/c-di-GMP

622 (gray) with SmbA$_{wt}$/(c-di-GMP)$_2$ (cyan) with RMSD of 0.4. Relevant secondary structure elements

623 are labeled. Dimeric c-di-GMP (cyan) and monomeric (thick) are shown as ball-and-stick models. **(b**

624 Superposition of SmbA$_{\Delta loop}$/c-di-GMP (gray) with SmbA/ppGpp (Magenta) with RMSD of

625 0.5. Relevant secondary-structure elements are labeled. ppGpp (magenta) and monomeric

626 (thick in gray) are shown as ball-and-stick models. The disordered part of loop 7 is marked

627 by broken lines. **(c)** AlphaFold2 predicted model of SmbA$_{wt}$ (yellow) with loop 7 is show in

628 green color. **(d)** Superposition of SmbA$_{wt}$/(c-di-GMP)$_2$ (green) with AlphaFold2 model of

629 SmbA$_{wt}$ (yellow). Loop 7 from SmbA$_{wt}$/(c-di-GMP)$_2$ and Alphfold model of SmbA$_{wt}$ Apo

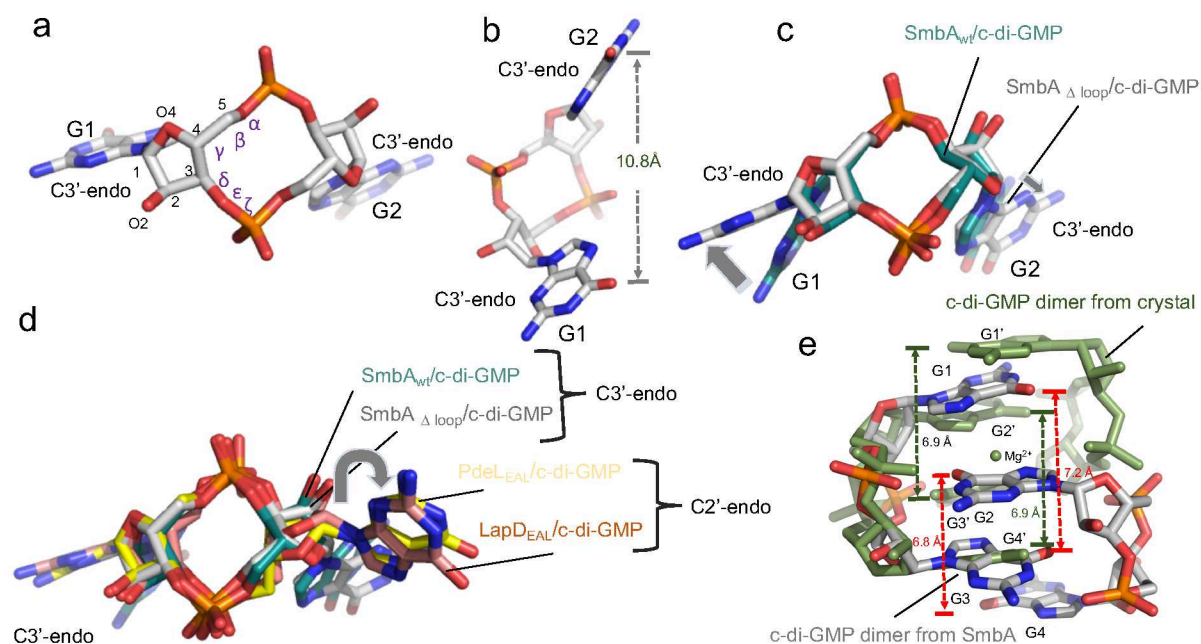**630** are show in red and green repectively.

631

632
633

Figure 6. Observed c-di-GMP conformations in SmbA$_{loop}$ and its comparison with SmbA$_{wt}$, PdeL and LapD. (a) and **(b)** shows the partial open-twisted form of monomeric c-di-GMP in C3'-endo sugar pucker conformation observed in SmbA mutant. Guanine distances are shown in black dotted line.

(c) Superimposition of c-di-GMP from SmbA$_{\Delta loop}$, SmbA$_{wt}$ and LapD$_{EAL}$. GMP moiety from both structures shows the same conformation, the C3'-endo sugar pucker; however, there are considerable differences in the G1 and G2 base orientation (indicated by the gray arrow). **(d)** Superimposition of c-di-GMP from SmbA$_{\Delta loop}$ with monomeric c-di-GMP as observed when bound to a phosphodiesterase PdeL and degenerated-phosphodiesterase LapD. Distinct sugar pucker of the base at the right (G2) appears responsible for the fully elongated form of c-di-GMP when bound to PdeL or LapD. In contrast, all bases at the left (G1) show the same sugar pucker, i.e. C3'-endo as also observed for SmbA$_{\Delta loop}$ in this study. (e) Superimposition of crystal structure of c-di-GMP/Mg^{2+54} and dimeric c-di-GMP from SmbA$_{wt}$. Guanine distances are shown in red and green dotted lines of c-di-GMP/ Mg^{2+} and dimeric c-di-GMP from SmbA$_{wt}$ respectevily.
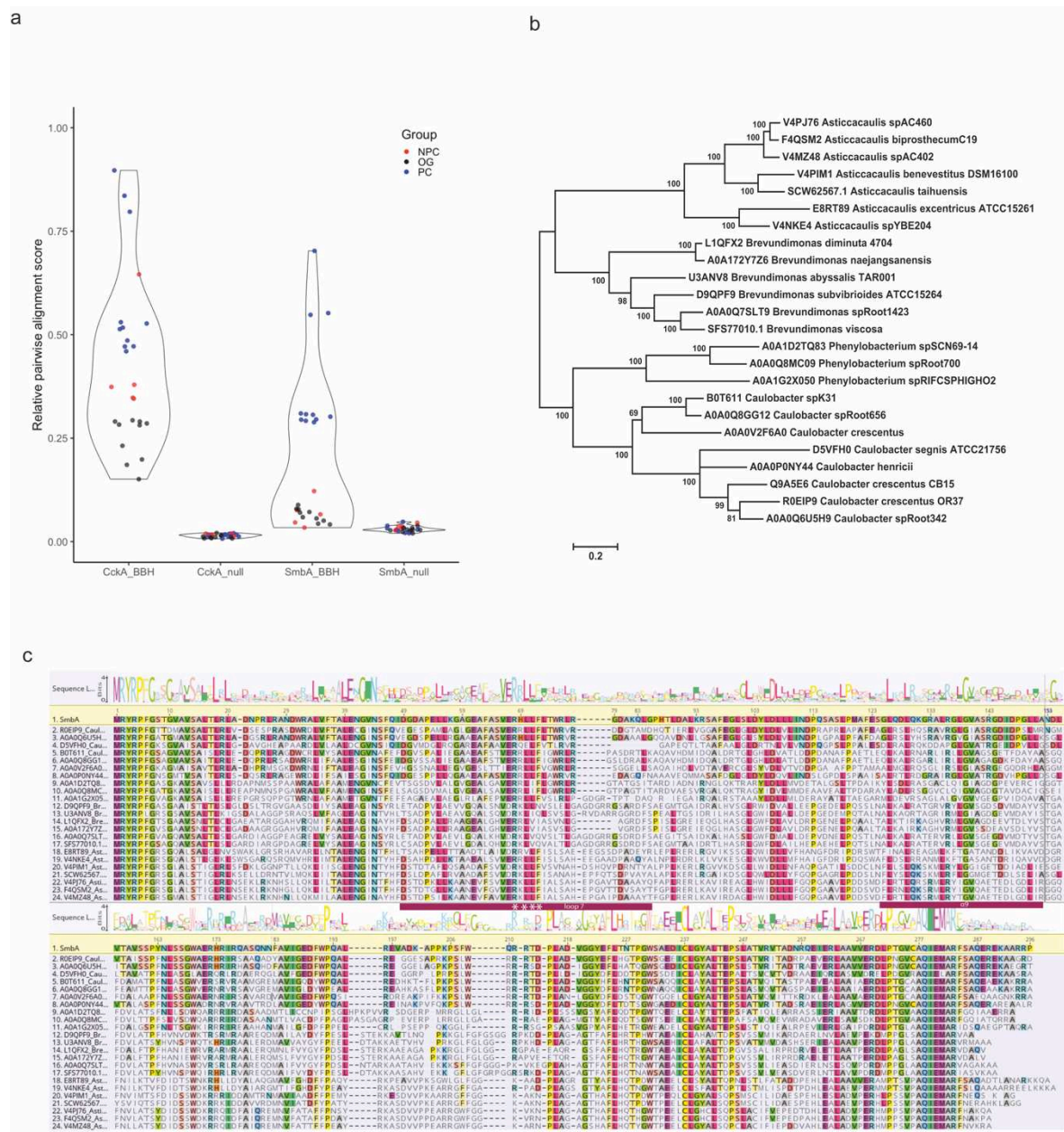
647
648

649

Figure 7. Sequence alignment and distance of SmbA homologs. (a) Pairwise Needleman-Wunsch global alignment scores of SmbA and CckA reciprocal best BLAST hits (BBH) for species sampled from prosthecate Caulobacterales (PC), non-prosthecate Caulobacterales (NPC), and other bacterial groups (OG). Alignment scores are reported relative to self-alignment of SmbA (Q9A5E6) and CckA (H7C7G9) from Caulobacter crescentus. For the null models, CckA BBH was scored against SmbA and vice versa. The latter BBH was identified using BLASTp against the NCBI-NR database using the BLOSUM45 scoring matrix. **(b)** A phylogenetic tree of 24 SmbA orthologs inferred using the Maximum Likelihood method based on the JTT model as implemented in MEGA7. Branch lengths indicate the number of substitutions per site. The tree with the highest log likelihood (-9134.38) is shown, with bootstrap support from 100 replicates indicated at branches. **(c)** Sequence alignment and logo of SmbA orthologs. The sequence logo was generated using the WebLogo server from the global alignment of SmbA orthologs used to build the distance tree.

662

Table 1. Crystallographic data collection and refinement statistics.

Data collection	SmbA$_{\Delta loop}$/c-di-GMP	SmbA$_{\Delta loop}$
Synchrotron source	SLS, PXIII	SLS, PXI
Wavelength (Å)	1.00004	1.00004
Space group	P 4$_3$ 2$_1$ 2	P 2$_1$
a, b, c (Å)	56.0, 56.0, 205.1	61.4, 208.1, 64.2
α, β, γ (°)	90, 90, 90	90, 117.6, 90
Resolution (Å)	21.5-1.4 (1.45-1.4) *	56.9-1.8 (1.87-1.8)
Unique reflections	65577 (6381)	128620 (12871)
Completeness	99.93 (99.87)	98.7 (97.9)
I/σ (I)	20.6 (2.6)	12.06 (2.9)
Redundancy	22.9 (22.9)	3.3 (3.3)
R$_{merge}$ (%)	9.8 (164)	7.4 (55.5)
R$_{pim}$ (%)	2.1 (352)	4.9 (36.1)
CC (1/2) %	99.9 (86.4)	99.6 (73.3)
Refinement		
R$_{work}$/R$_{free}$ (%)	14.8/17.7	16.8/20.3
RMSD		
Bond lengths (Å)	0.006	0.009
Bond angles (°)	0.9	1.05
Molecules/asymmetric unit	1	4
No. of atoms		
Protein	2081	8952
Ligand	99	0
Water	299	1265
Average B-factor (Å^2)	20.4	24.0
Protein	18.5	22.7
Ligand	21.4	
Water	33.3	33.6
Ramachandran statistics (%)		
Favored regions	99.25	98.26
Allowed regions	0.75	1.74
Disallowed regions	0.0	0.0
Deposition		
PDB codes	7B0E	8BVB

664   (* = The values recorded in parentheses are those for the highest resolution shell)

665

666

667

668